NATIONAL ADVISORY COMMITTEE FOR AERONAUTICS

TECHNICAL NOTE 2308

VIBRATORY STRESSES IN PROPELLERS OPERATING IN THE FLOW FIELD OF A WING-NACELLE-FUSELAGE COMBINATION

By Vernon L. Rogallo, John C. Roberts, and Merritt R. Oldaker

Ames Aeronautical Laboratory
Moffett Field, Calif.

Washington
March 1951

NATIONAL ADVISORY COMMITTEE FOR AERODYNAMICS

TECHNICAL NOTE 2308

VIBRATORY STRESSES IN PROPELLERS OPERATING IN THE FLOW FIELD OF A WING–NACELLE–FUSELAGE COMBINATION

By Vernon L. Rogallo, John C. Roberts, and Merritt R. Oldaker

SUMMARY

An investigation has been made to determine the first–order vibratory stresses induced in propellers of conventional design when rotating in the flow field of a wing–nacelle–fuselage combination, and to thus enable careful evaluation of the steps essential to the prediction of these stresses. Thrust measurements were obtained by means of propeller–wake surveys in order to define the magnitude of the force changes (the oscillating air loads) experienced by the blades. Stress measurements were made simultaneously to obtain the propeller response to the oscillating air loads. Three– and four–blade, hollow, steel propellers having diameters of approximately 13 feet were used in the investigation.

Two significant conclusions may be drawn regarding the accuracy of existing methods of predicting the oscillating air loads on, and the resultant first–order vibratory stresses in the propellers. Steady–state propeller theory was adequate for the prediction of the magnitude and distribution of the oscillating air loads, provided the known complete flow–field characteristics were used. With the known oscillating air load, an accurate prediction of nonresonant, first–order vibratory stresses was obtained. These two conclusions are believed to be applicable to propellers of conventional design for low blade–angle settings, provided that the blades are unstalled and supercritical speeds are not encountered.

INTRODUCTION

The rotation of a propeller (inclined or noninclined) in an unsymmetrical flow field results in oscillating air loads on the blades. Unsymmetrical flow fields have been found to be present at the propeller plane for wing–nacelle–fuselage combinations. Of particular concern is

that component of the oscillating air loads induced by such unsymmetrical flow fields which completes one cycle (wave form approximately sinusoidal) for each revolution of the propeller blade. This oscillating air load and the associated vibratory stresses are termed first order. The magnitude of the stresses can be quite high even when the frequency of the vibration is far remote from resonance.

Existing methods of computation have not always satisfactorily accounted for the first-order vibratory stresses measured during flight investigations. This may have been due either to inherent inaccuracies of the methods themselves, or a lack of exact knowledge of operating conditions, or both. In order to provide experimental data suitable for use in evaluating the methods of stress prediction, an investigation was made in the Ames 40- by 80-foot wind tunnel wherein complete instrumentation and precise control of operating conditions could be obtained.

Data were obtained for evaluating the procedure of each of the following three steps which are necessary in predicting first-order vibratory stresses:

1. Computation of the characteristics of the flow field

2. Computation of the air-load variation on the propeller operating in this flow field

3. Computation of the stresses due to this air-load variation

In order to obtain the necessary information for step 1, stream-angle and velocity surveys were made at the propeller plane before installing the propeller. With the propeller installed, thrust and stress measurements were made to provide the necessary information to evaluate the procedure of steps 2 and 3.

Comparisons have been made of experimental and predicted results for all steps. The comparisons of flow-field results are given in reference 1. Presented herein are comparisons of predicted and experimental air-load distributions and predicted and experimental stress distributions.

NOTATION

A blade cross-sectional area, square inches

b blade-section chord (basic airfoil), inches

b_s extension of blade-section chord, inches

b_t total blade-section chord (basic airfoil plus extension), inches

c_{l_d} design section lift coefficient (basic airfoil)

c_t section thrust coefficient $\left(\frac{\text{section thrust}}{\rho n^2 D^4}\right)$

Δc_t value of the section thrust coefficient at any angular position minus the value at the zero angular position

d_c distance from blade-section neutral axis to extreme fiber on camber surface (upper surface), inches

d_t distance from blade-section neutral axis to extreme fiber on thrust surface (lower surface), inches

D propeller diameter, feet

h blade-section thickness, inches

h_c ordinate measured from the chord line of the basic airfoil to the camber surface of a section, inches

h_t ordinate measured from the chord line of the basic airfoil to the thrust surface of a section, inches

I_{max} moment of inertia (maximum) of an entire section about an axis passing through the section centroid in the plane of the section, perpendicular to the chord line, inches^4

I_{min} moment of inertia (minimum) of an entire section about an axis passing through the section centroid in the plane of the section, parallel to the chord line, inches^4

N propeller rotational speed, revolutions per minute

n propeller rotational speed, revolutions per second

r radius to any blade section, inches

R tip radius, inches

t_c skin thickness, camber surface, inches

t_t skin thickness, thrust surface, inches

V_o free-stream velocity, miles per hour

x fraction of tip radius (r/R)

Y_{cg} distance, measured perpendicularly, from chord line of basic airfoil to centroid of the section, inches

Y_s distance, measured perpendicularly, from chord line of basic airfoil to center of trailing-edge radius of the extended section, inches

α_G geometric angle of attack of the airplane thrust axis, degrees

β section blade angle, degrees

ρ mass density of air, slugs per cubic foot

Ω angular position about the thrust axis, measured counterclockwise from the upper vertical position as viewed from the front, degrees

APPARATUS AND METHODS

Test Airplane and Propellers

The twin-engine, fighter-type airplane used for the investigation is shown in figure 1. The size and location of the propeller disk relative to the components of the airplane, as well as the principal dimensions of the airplane, are shown in figure 2. In order to provide precise control of operating conditions during the test and also to avoid engine-excited propeller vibrations, the reciprocating engine in the port nacelle was replaced by a 1500-horsepower electric motor. This change necessitated moving the propeller plane forward, as shown in figure 2. Only the port nacelle was instrumented for the investigation.

Three- and four-blade, hollow, steel propellers of Curtiss blade design 744-1C2-0 having diameters of 13 feet 2 inches were used in the investigation. The blade-form curves and section properties of the test propellers are presented in figures 3 and 4, respectively.

Instrumentation

The propeller blades were instrumented with Baldwin-Southwark, type SR-4-AD7, wire strain gages. Since first-order propeller vibrations occur as flatwise bending (bending about an axis parallel to the chord lines), the gages were located along the maximum thickness line of the blade with the axis of the gages parallel to the centroidal axis of the blade. Only one of the blades of each propeller was fully instrumented with strain gages as shown in figures 5(a) and 5(b). The strain-gage locations

shown in figure 5(b) are those used when the four-blade propeller was tested. For tests of the three-blade propeller, four additional gages were placed on the camber surface to provide a gage spacing of 3 inches from blade station 18 to blade station 42. All other blades were provided with gages on the shank and over the anticipated maximum-stress region of the blade on the camber surface so that the phase relationship between blades could be obtained. Remotely controlled switches, located forward of the propeller hub (fig. 5(c)), enabled rapid recording of the output signals of 40 electrical strain gages at any propeller operating condition. An individual bridge circuit, which included three fixed resistors located adjacent to the switches (fig. 5(c)), was provided for each strain gage. The power for the bridge circuits was transmitted through the Curtiss pitch control (brush and slip-ring assembly) and the gage output signals were transmitted through silver slip rings and silver graphite brushes to the recorder.

The output signals of the gages were recorded directly, without amplification, by a Consolidated 24-channel, moving-coil-type oscillograph with type 7-115 galvanometers attenuated with approximately 180 ohms damping resistance.

The propeller rotational speed and blade angular position were indicated by timing lines and pulses on the oscillograph record. One pulse occurred per revolution. It was produced by the voltage induced in a fixed coil by the passage of a small alnico magnet attached to the silver slip-ring assembly.

The rakes for surveying the propeller wake were located 8 inches aft of the propeller plane and were spaced at 45° increments around the nacelle. (See figs. 1 and 6.) Each rake consisted of seven shielded total-head tubes spaced radially at 8-inch intervals. The pressure measurements were indicated on a multiple-tube manometer board and were photographically recorded.

Calibration of Strain-Gage Instrumentation

The strain-gage factors were determined by statically loading a blade, measuring the strains at each gage position with a Tuckerman (optical-type) strain gage, and simultaneously recording the local resistance-gage output indicated by a sensitive galvanometer. The gage factors were found to be within the values specified by the manufacturer. The measured strains were found to be in good agreement with those obtained by calculations using the known blade-section properties, except in the region of highest strain where local deformation occurred. The galvanometer elements were calibrated individually in order to obtain both frequency response and phase characteristics. The sensitivity of the system, galvanometer displacement for a given resistance change, was checked periodically during the tests. This was accomplished by statically unbalancing

the bridge circuits with precision resistors, and recording the resulting galvanometer displacements. Dynamic calibration of the system was also made by exciting the propeller with electronic vibration equipment at controlled frequencies and amplitudes.

TEST CONDITIONS

The various test conditions are given in the following table:

Variable	$\beta_{0.75R}$ (deg)	α_G (deg)	V_o (mph)	N (rpm)
Propeller speed	20	10	75	410 to 805
	20	10	140	810 to 955
	20	8	165	960 to 1250
	12.5	10	100	670 to 1250
Angle of attack	20	-2 to 8	165	1090, 1175, 1265
Free stream velocity	20	6	0 to 173	1010
	12.5	10	0 to 138	1250

Because of model-power, tunnel-airspeed, and tunnel-balance-load limitations, the propeller could not be operated over the entire rotational-speed range for all angles of attack and tunnel airspeeds.

REDUCTION OF DATA

Analysis of Stress Records

Since the recording galvanometers and the complete strain-gage system were calibrated, the stresses were directly obtained from the oscillographic traces. These traces were relatively free from external disturbances and remained periodic during the recording at specific propeller operating conditions. The vibration oscillations included not only first-order (once per revolution, or 1P), but also second-order (twice per revolution, or 2P) oscillations. The components were readily separated by use of the method of superposition described in reference 2.

Analysis of Propeller Wake-Survey Data

The thrust coefficients were computed from wake surveys by the method given in reference 3. This method required measurements of total-head pressure immediately aft of the propeller plane in the absence of the propeller and in the presence of the propeller. Previous work (references 3 and 4) has shown this method to be an acceptable means of measuring thrust.

RESULTS AND DISCUSSION

The results of this investigation, which provide the necessary information for evaluating steps (2) and (3) in the prediction of first-order vibratory stresses, will be presented in the following manner. Typical air-load measurements will be presented and the evaluation of the method of computation of the air load will follow. Typical stress results will then be presented and the evaluation of the method of computation of the stress will follow. Most of the results presented are for the four-blade propeller since they are generally representative of those for the three-blade propeller, except as will be noted. The effect of the blade instrumentation on the air loads and resultant stresses is believed to be small since the agreement in magnitude of the blade stresses for the fully instrumented blade and the blades of limited instrumentation was within the accuracy of the measurements.

Oscillating Air Loads

The aerodynamic excitation of a propeller (inclined or noninclined) results from the change in blade normal force incurred during a revolution of the propeller. Since the thrust is a direct function of the normal force, the thrust change may be used as a measure of the oscillating air load. Hereinafter thrust will be referred to as air load, and for convenience the coefficient form c_t will be used.

Measured air loads.- Typical values of the measured air loads are presented in figure 7 wherein the section thrust coefficient c_t is plotted as a function of the angular position Ω around the disk for one set of test conditions for the four-blade propeller installation. These results were not corrected for slip-stream rotation which primarily affects the position of the air load with respect to Ω, but has little effect on the measured magnitude of the air load. It may be noted that the wave-form characteristics of the oscillating air loads for each of the various blade stations are quite similar and that the respective maximum and minimum thrust values occur at very nearly the same angular position. Similar results were obtained at other propeller operating conditions for both the three- and four-blade propeller installations.

Comparison of measured and predicted air loads.- The method used for predicting the oscillating air loads (reference 1) was derived from a propeller theory based on steady-state conditions. The flow-field data of reference 1 were used for the computations. Figure 8(a) shows a comparison of the measured and the computed variations of the incremental section thrust coefficient Δc_t with angular position Ω. The comparisons are for a blade section at the 0.7-radius stations of the propeller. The component parts of the measured and calculated air loads are shown in figure 8(b). The principal component is first-order (1P) and the remainder, second-order (2P). (In fig. 8(b), to enable

better comparison, the curves for each component of both experimental and predicted air-load variations have been displaced vertically so that they have a mean value of zero; hence, the addition of the respective components would result in wave forms identical in shape but vertically displaced from those shown in fig. 8(a).) The adequacy of the method of computation is demonstrated by the agreement as to both magnitude and wave form. No attempt is made to account for the phase difference between the measured and computed variations since it is only the magnitude of the air loads which are of concern in the prediction of the stresses.

Excellent agreement was also obtained for other blade stations. This is indicated in figure 9, which compares the computed and measured distributions of the maximum variations of the first-order incremental section thrust coefficient. The measured results were reduced from the data presented in figure 7. These plots are typical of those used in the computation of the first-order air-load bending moments. It may be concluded from the comparisons presented in figures 8 and 9 that steady-state propeller theory is adequate for the prediction of the oscillating air loads.

Vibratory Stresses

Measured Stresses.- The term "total stress" will be used in this report to designate one-half the vibratory stress fluctuation indicated by the wave forms on the oscillograph records. As previously noted, the total stress was composed of both first- and second-order stresses. The values of total stress as well as the first- and second-order stress components are presented where appropriate.

The effects of the test variables on vibratory stress are presented in figures 10 to 13, inclusive. The effect of propeller rotational speed for the four-blade propeller is shown in figures 10 and 11. The data of figure 10 are for the 24-inch blade station which was near the region of maximum stress, and those of figure 11 are for the blade shank. The curves (fig. 10) are discontinuous because of the previously mentioned limitations on operating conditions. (See section entitled "Test Conditions.") The effect of thrust-axis inclination on the stresses measured at the 24-inch-radius station of the propeller is shown in figure 12, and the effect of forward velocity is shown in figure 13. In obtaining the data all factors and variables were held constant except one, the effects of which were being studied. It may be noted in figures 10(b) and 11 that the first-order stress component increased uniformly with propeller rotational speed. This characteristic was expected even in the absence of resonance since the air load increased with rotational speed. Stress predictions (shown later) based on nonresonant conditions for the highest rotational speeds encountered during the test indicate the conditions to be far remote from resonance. The variation of first-order vibratory stress with thrust-axis inclination is shown in figure 12 to be linear.

The variation of first-order vibratory stress with forward velocity is shown in figure 13 to be approximately linear over the speed range tested. Although the stress variations shown are for two selected blade stations, in general, they are typical for other blade stations.

Two occurrences of resonance in the second-order vibration pattern were found for the four-blade propeller and are indicated in figure 10(c). The first occurred at approximately 475 rpm and the second at approximately 1175 rpm. The phase relations between blades and the stress distributions indicated that the two modes were, respectively, the fundamental reactionless mode in flatwise bending, and the fundamental reactionless mode in edgewise bending. The stress peak resulting from the latter resonant condition is quite apparent from the shank stress measurements (fig. 11). In neither case of second-order resonance was there a measurable effect on first-order stress at either the 24-inch blade station or the blade shank. A reactionless mode cannot be excited in a propeller having three blades; hence the second-order characteristics found for the three-blade propeller were somewhat different from those obtained for the four-blade propeller. In the case of the three-blade propeller, only one condition of resonance was encountered during the tests. The mode was identified as the unsymmetrical fundamental mode and was excited at a rotational speed of 460 rpm.

Comparison of computed and measured stress distributions.- The computed stresses presented in this report were obtained by use of the integration method developed by the Propeller Division of the Curtiss-Wright Corporation (reference 5). The basic assumptions of the method are that the vibration is nonresonant, the oscillating air load variation is sinusoidal, and the blade is not twisted and has a blade angle equal to that of the blade section about which the major part of the blade tends to deflect. Estimates of blade aeroelastic twist for the maximum stress loadings indicated such twist to be negligible and therefore the effects of twist were omitted in the stress computations.

The oscillating air load variations used in the stress computations were obtained from theoretical computations; however, either theoretical or experimental air load distributions could have been used since the magnitude of the loadings were in good agreement.

Comparisons of computed and measured stress distributions are presented in figures 14 and 15. The comparisons in figures 14(a) and 14(b) are for test conditions at which the highest 1P stresses were encountered for the four-blade propeller at blade-angle settings of 20° and 12-1/2°, respectively. The comparison presented in figure 15 is for the three-blade propeller when operating at the same test conditions as given in figure 14(a). The higher magnitude of the stresses for the three-blade propellers is due to greater aerodynamic loading per blade resulting from lower propeller-induced flow angles.

Good agreement for all comparisons may be noted for all radial locations except in the region of highest stress. The slight disagreement found here is believed due to local deformation, characteristic of hollow-steel propellers without internal stiffeners. Such disagreement was noted between computed and measured stresses for a static loading condition of the propeller.

CONCLUSIONS

Two significant conclusions may be drawn regarding the accuracy of existing methods of predicting the oscillating air loads on, and the resultant first-order vibratory stresses in the investigated propellers. These two conclusions, which are believed to be applicable to conventional propellers when operating with low blade-angle settings below stall and supercritical speeds, are as follows:

1. Steady-state propeller theory was adequate for the prediction of the magnitude and distribution of the oscillating air loads, provided the complete flow-field characteristics were known.

2. With the known oscillating air load, an accurate prediction of nonresonant, first-order vibratory stresses was obtained.

Ames Aeronautical Laboratory,
National Advisory Committee for Aeronautics,
Moffett Field, Calif., Dec. 8, 1950

REFERENCES

1. Roberts, John C., and Yaggy, Paul F.: A Survey of the Flow at the Plane of the Propeller of a Twin-Engine Airplane. NACA TN 2192, 1950.

2. Manley, R. G.: Wave Form Analysis. John Wiley & Sons, Inc., N.Y., 1945.

3. Reid, Elliott G.: Wake Studies of Eight Model Propellers. NACA TN 1040, 1946.

4. Pendley, Robert E.: Effect of Propeller-Axis Angle of Attack on Thrust Distribution Over the Propeller Disk in Relation to Wake-Survey Measurement of Thrust. NACA ARR L5J02b, 1945.

5. Stulen, F. B., and DeVries, J. A.: Calculation of the First-Order Vibratory Propeller Blade Stresses by the Integration or Simplified Matrix Method. Report C-2132, Curtiss-Wright Corp., Propeller Div., (Caldwell, N. J.), Jan. 27, 1950.

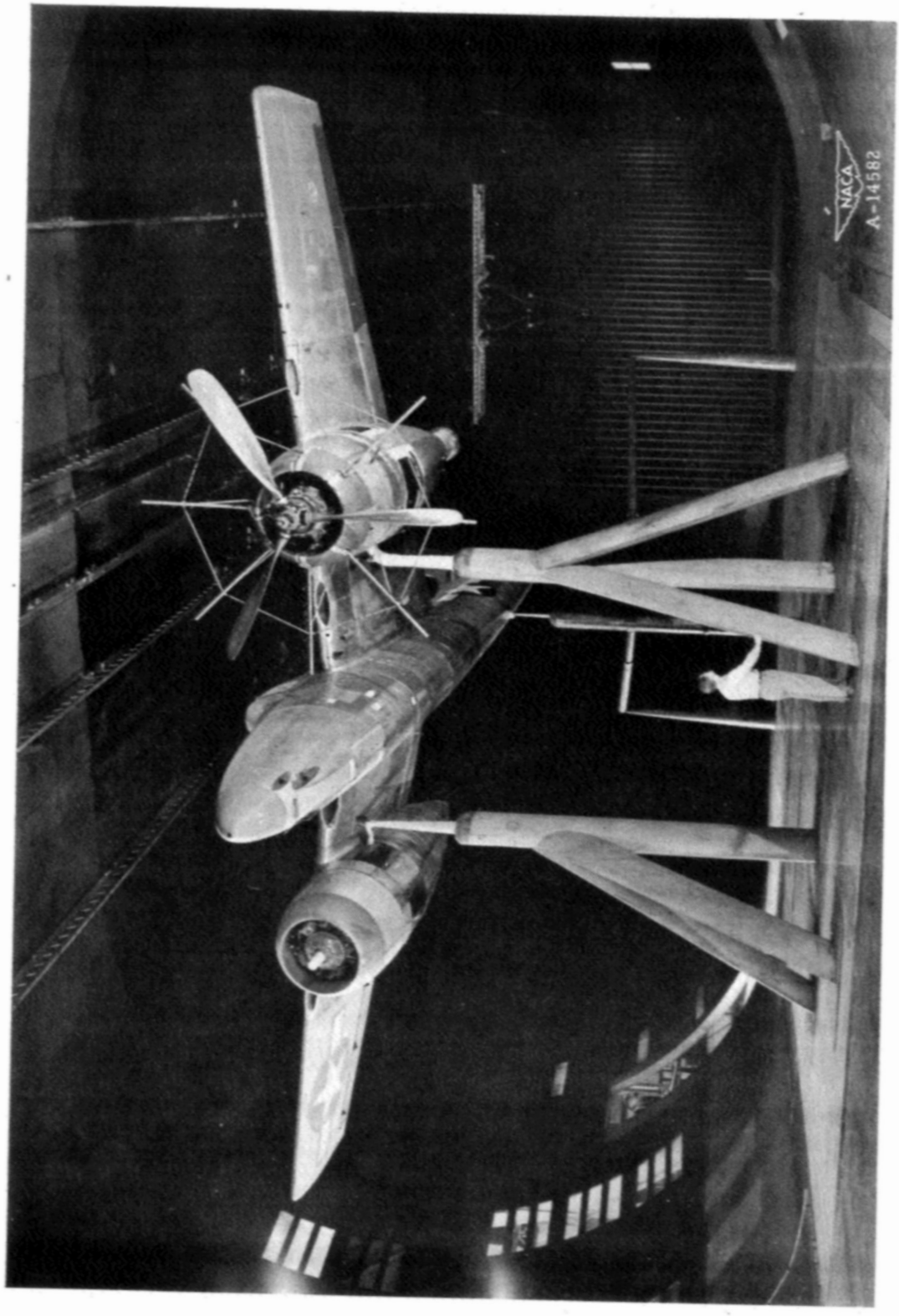

Figure 1.- The airplane mounted in the Ames 40- by 80-foot wind tunnel.

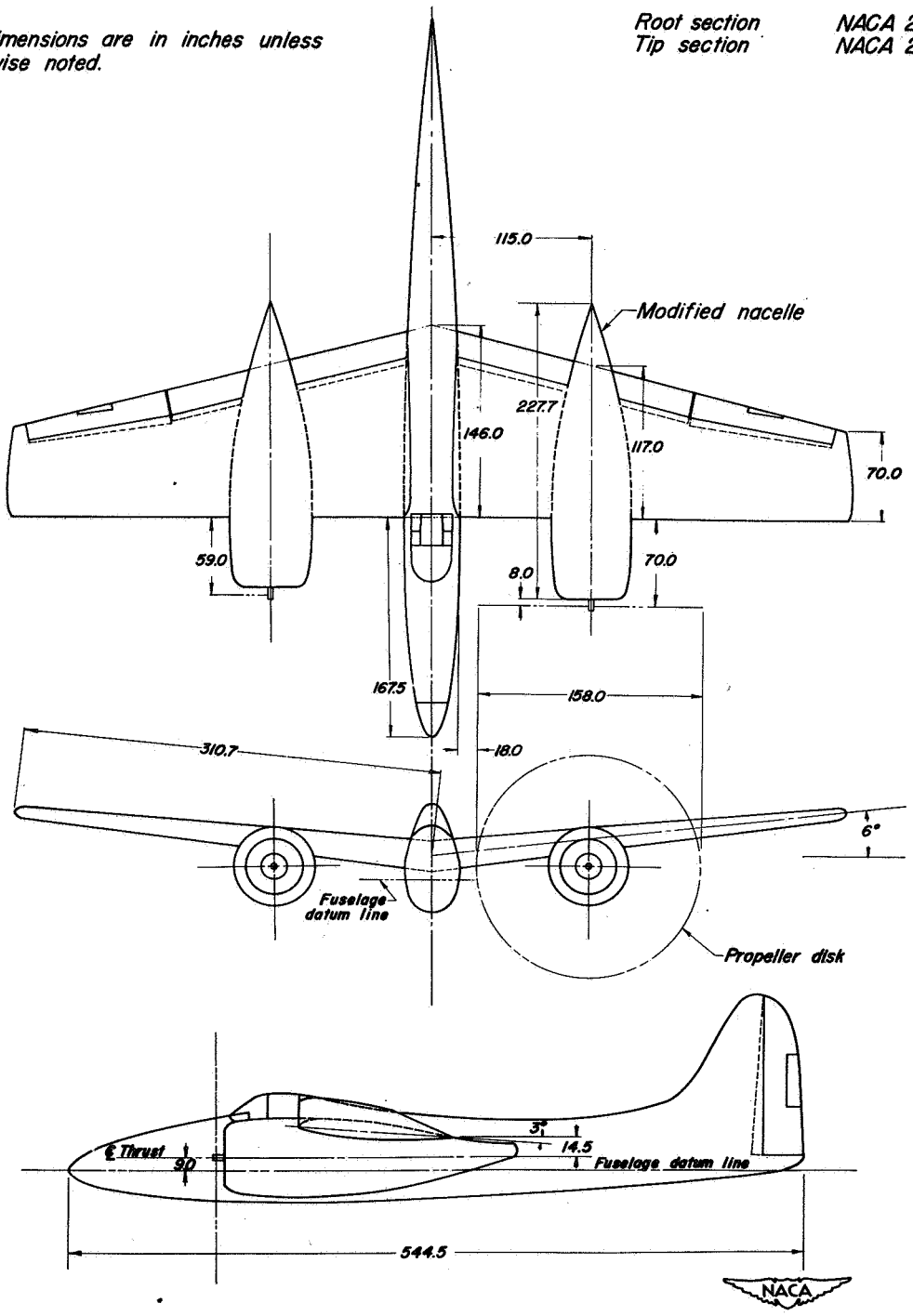

Figure 2.- Geometric characteristics of the twin-engine, fighter-type airplane.

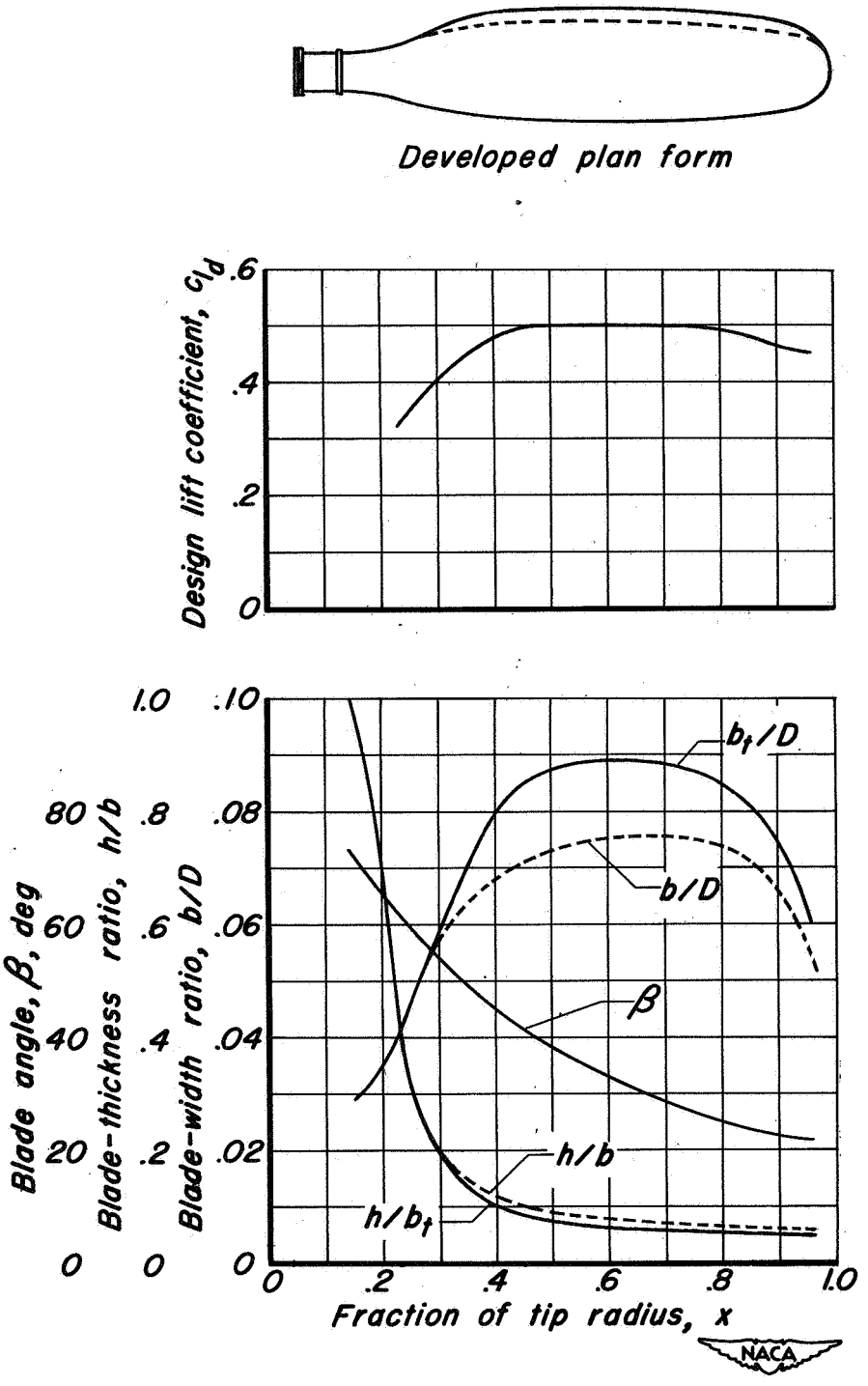

Figure 3. - Blade-form curves for the test propellers, Curtiss type 744-IC2-0. Diameter, 13 feet, 2 inches.

Typical blade section

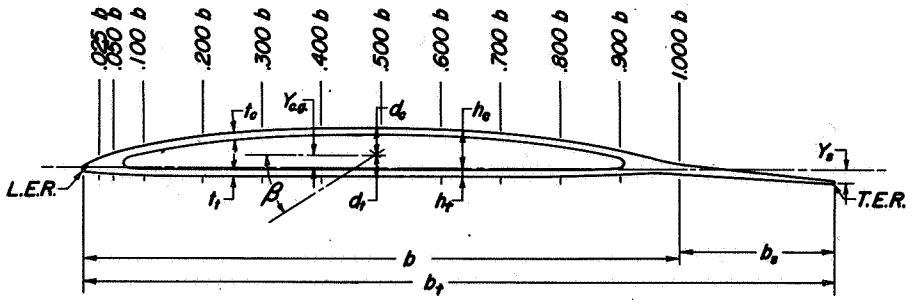

Blade-section properties

Radius / Symbol	11.75	13	19	25	31	37	43	49	55	61	67	73	76
A	3.861	3.764	3.217	2.799	2.583	2.317	2.133	2.394	2.620	2.503	2.369	2.057	1.684
β		70.20	59.85	51.90	45.35	40.00	35.65	32.00	28.85	26.25	23.95	22.10	21.30
b_g		0	0	.25	1.61	1.94	1.96	1.94	1.89	1.78	1.64	1.36	1.02
b_t		4.640	6.980	9.730	12.390	13.230	13.700	13.870	13.860	13.560	12.920	11.300	9.310
b_t/D	.0290	.0297	.0447	.0623	.0794	.0854	.0878	.0869	.0889	.0869	.0828	.0724	.0597
h/b_t	1.000	.924	.340	.167	.101	.078	.068	.063	.061	.057	.054	.050	.049
d_o	2.265	2.141	1.134	.751	.520	.398	.337	.298	.278	.255	.234	.197	.164
d_t	2.265	2.145	1.239	.878	.726	.626	.595	.580	.564	.522	.472	.385	.302
I/d_o	3.850	3.608	1.958	1.174	.892	.736	.665	.748	.752	.710	.581	.386	.262
I/d_t	3.850	3.601	1.792	1.005	.639	.461	.376	.384	.371	.347	.288	.197	.142
I_{min}	8.721	7.724	2.220	.882	.464	.293	.224	.223	.209	.161	.126	.076	.043
I_{max}	8.72	8.77	12.81	23.42	32.74	34.06	32.58	35.30	36.15	33.54	28.95	18.55	8.15
t_o		.287	.215	.137	.103	.085	.074	.081	.088	.084	.081	.078	.077
t_t		.287	.215	.137	.103	.085	.074	.094	.113	.108	.104	.101	.099
T.E.R.		1.995	.323	.042	.023	.020	.020	.020	.020	.020	.020	.020	.020
L.E.R.		1.995	.448	.137	.070	.046	.036	.032	.028	.025	.021	.020	.020
Y_{og}		.008	.077	.138	.165	.207	.209	.208	.206	.198	.181	.140	.112
Y_g		0	0	.026	.169	.204	.206	.204	.199	.187	.172	.143	.107

Blade coordinates

$r/_D$	Radius / b	13	19	25	31	37	43	49	55	61	67	73	76
2.5	h_o	.672	.397	.300	.246	.216	.200	.192	.187	.175	.159	.133	.106
2.5	h_t	.668	.337	.197	.133	.098	.083	.074	.066	.058	.050	.035	.025
5	h_o	.936	.556	.420	.351	.312	.292	.282	.275	.258	.237	.197	.158
5	h_t	.931	.466	.268	.174	.123	.100	.087	.079	.066	.051	.035	.024
10	h_o	1.289	.768	.585	.500	.449	.423	.410	.400	.377	.347	.289	.233
10	h_t	1.279	.637	.360	.222	.149	.116	.099	.082	.065	.049	.033	.023
20	h_o	1.721	1.035	.799	.695	.631	.597	.580	.568	.536	.493	.413	.332
20	h_t	1.706	.843	.471	.276	.174	.129	.104	.083	.064	.047	.030	.021
30	h_o	1.972	1.197	.933	.817	.745	.705	.686	.675	.635	.586	.490	.395
30	h_t	1.954	.967	.540	.309	.190	.136	.107	.085	.063	.044	.027	.019
40	h_o	2.109	1.287	1.010	.886	.810	.768	.747	.736	.692	.638	.534	.431
40	h_t	2.089	1.034	.580	.330	.199	.142	.109	.085	.062	.041	.024	.017
50	h_o	2.153	1.316	1.036	.910	.831	.789	.767	.756	.711	.655	.547	.441
50	h_t	2.133	1.057	.593	.336	.203	.143	.111	.086	.061	.038	.021	.015
60	h_o	2.109	1.285	1.007	.884	.808	.766	.746	.736	.691	.637	.533	.430
60	h_t	2.089	1.033	.577	.328	.198	.140	.108	.084	.060	.036	.018	.013
70	h_o	1.971	1.185	.913	.801	.732	.694	.675	.670	.629	.575	.483	.389
70	h_t	1.953	.954	.519	.294	.177	.125	.096	.078	.056	.034	.015	.011
80	h_o	1.719	.999	.736	.646	.591	.561	.546	.551	.520	.466	.386	.314
80	h_t	1.704	.805	.407	.227	.134	.092	.072	.061	.048	.032	.012	.009
90	h_o	1.286	.691	.453	.400	.367	.349	.353	.366	.343	.303	.237	.196
90	h_t	1.276	.570	.248	.138	.080	.054	.043	.039	.032	.022	.009	.007
100	h_o			.083	.083	.073	.066	.063	.063	.063	.063	.061	.057
100	h_t			.083	.083	.073	.066	.063	.063	.063	.063	.061	.057

NACA

Figure 4. - Blade-section properties for the test propeller, Curtiss type 744-IC2-0. Diameter, 13 feet, 2 inches.

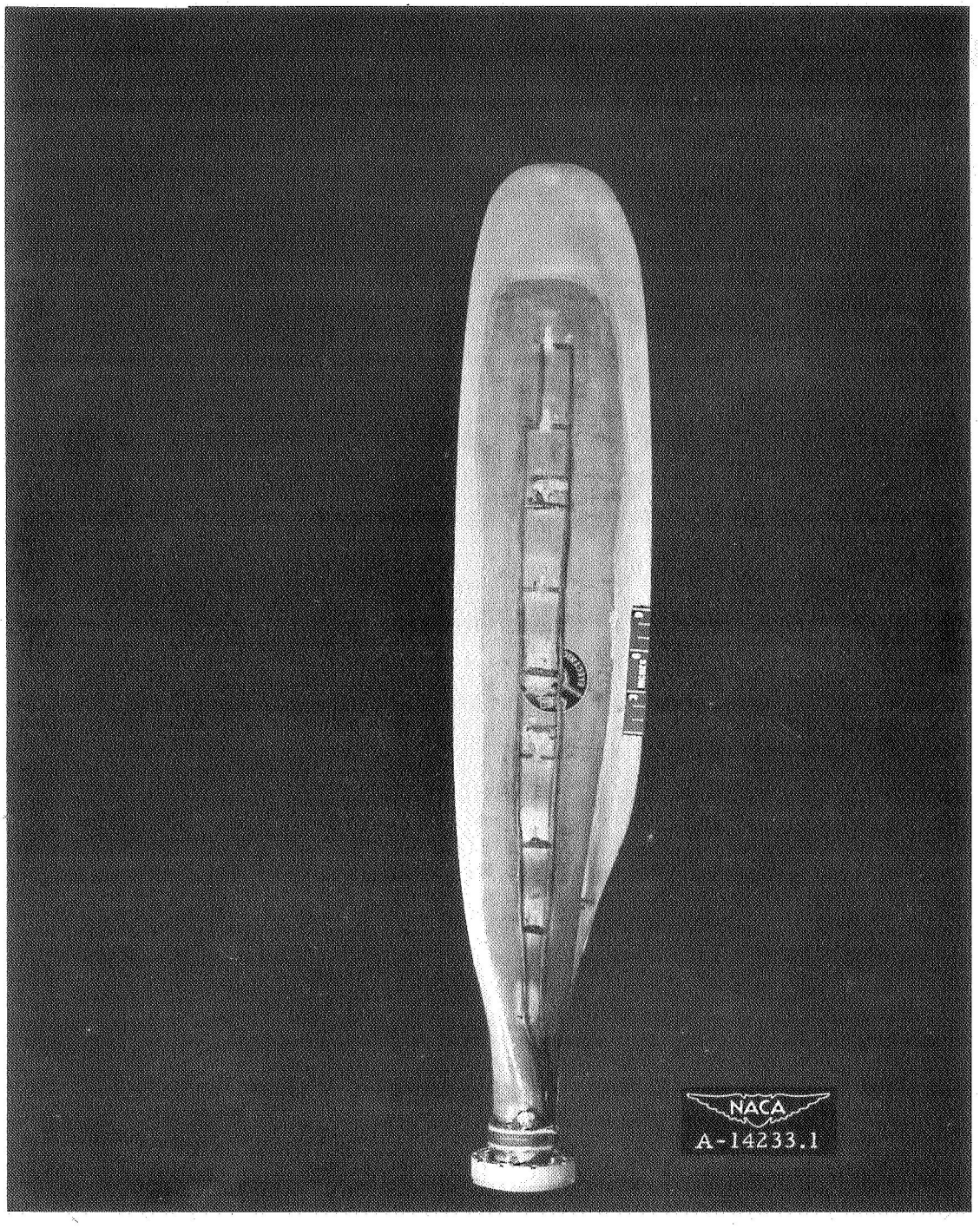

(a) Camber surface of fully instrumented blade.

Figure 5.- Instrumentation of test propeller.

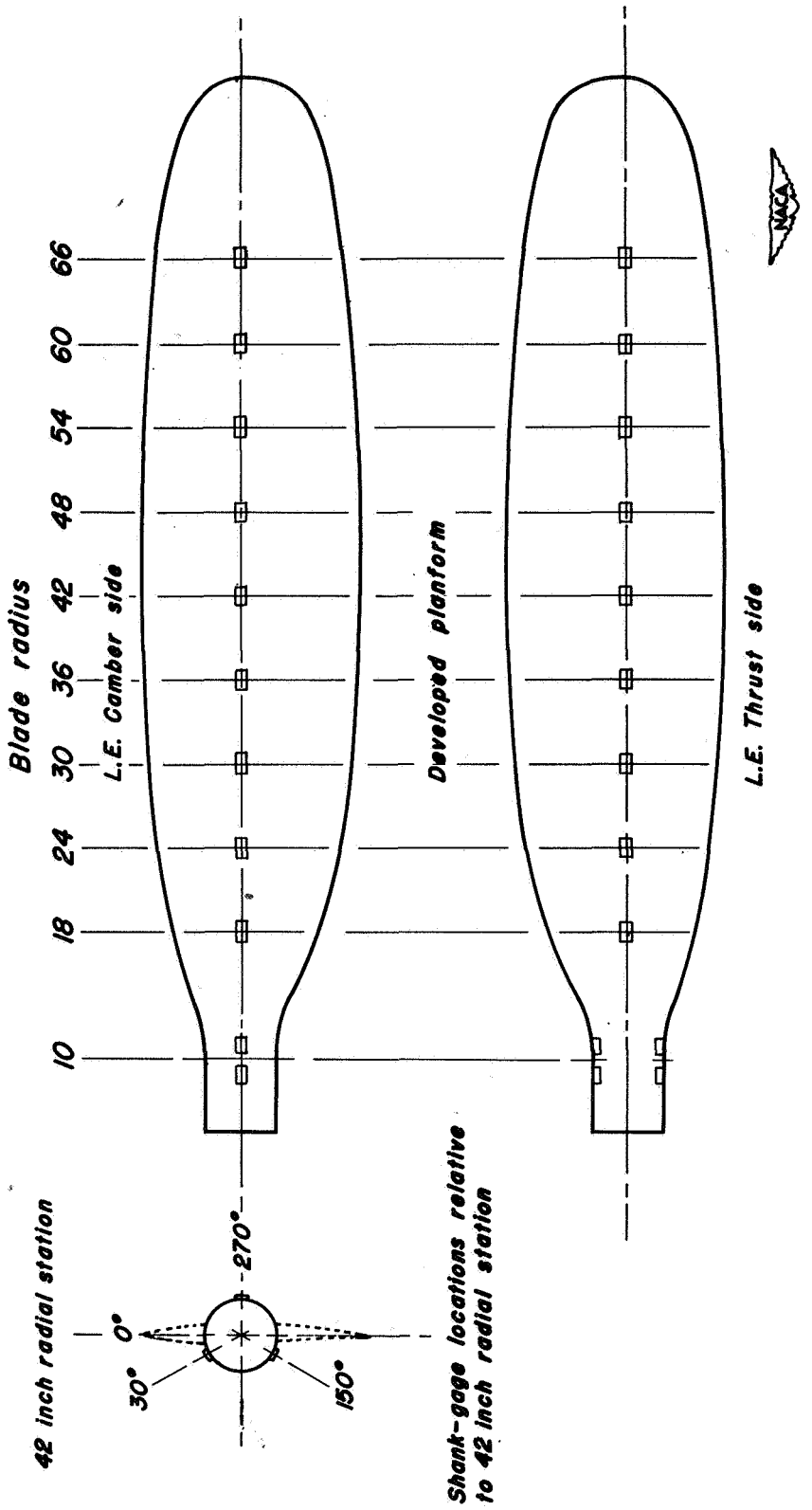

(b) Strain-gage location on fully instrumented blade

Figure 5.- Continued.

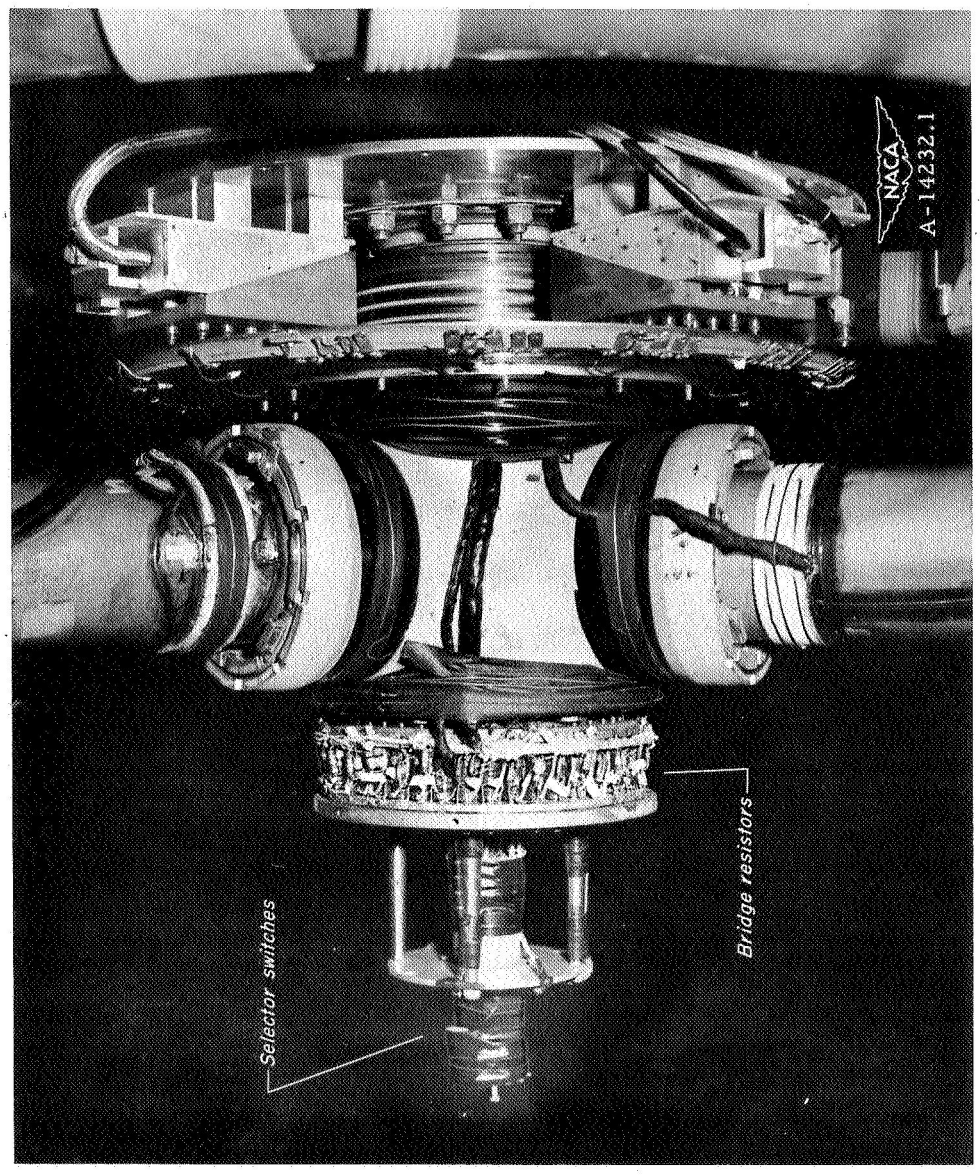

(c) Gage selector switches, bridge resistors, slip rings, and brush assemblies.

Figure 5.- Concluded.

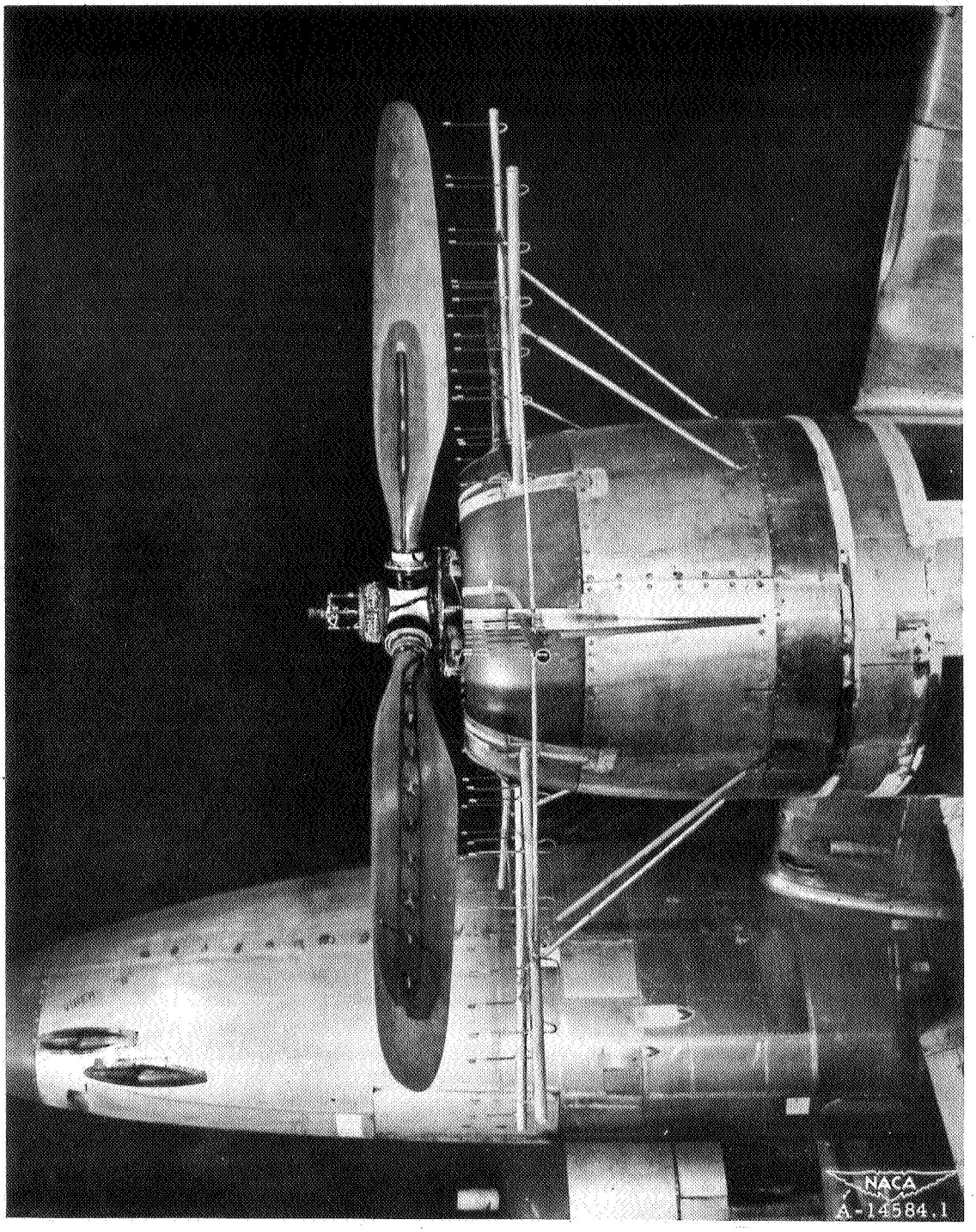

Figure 6.- Propeller wake-survey rake installation.

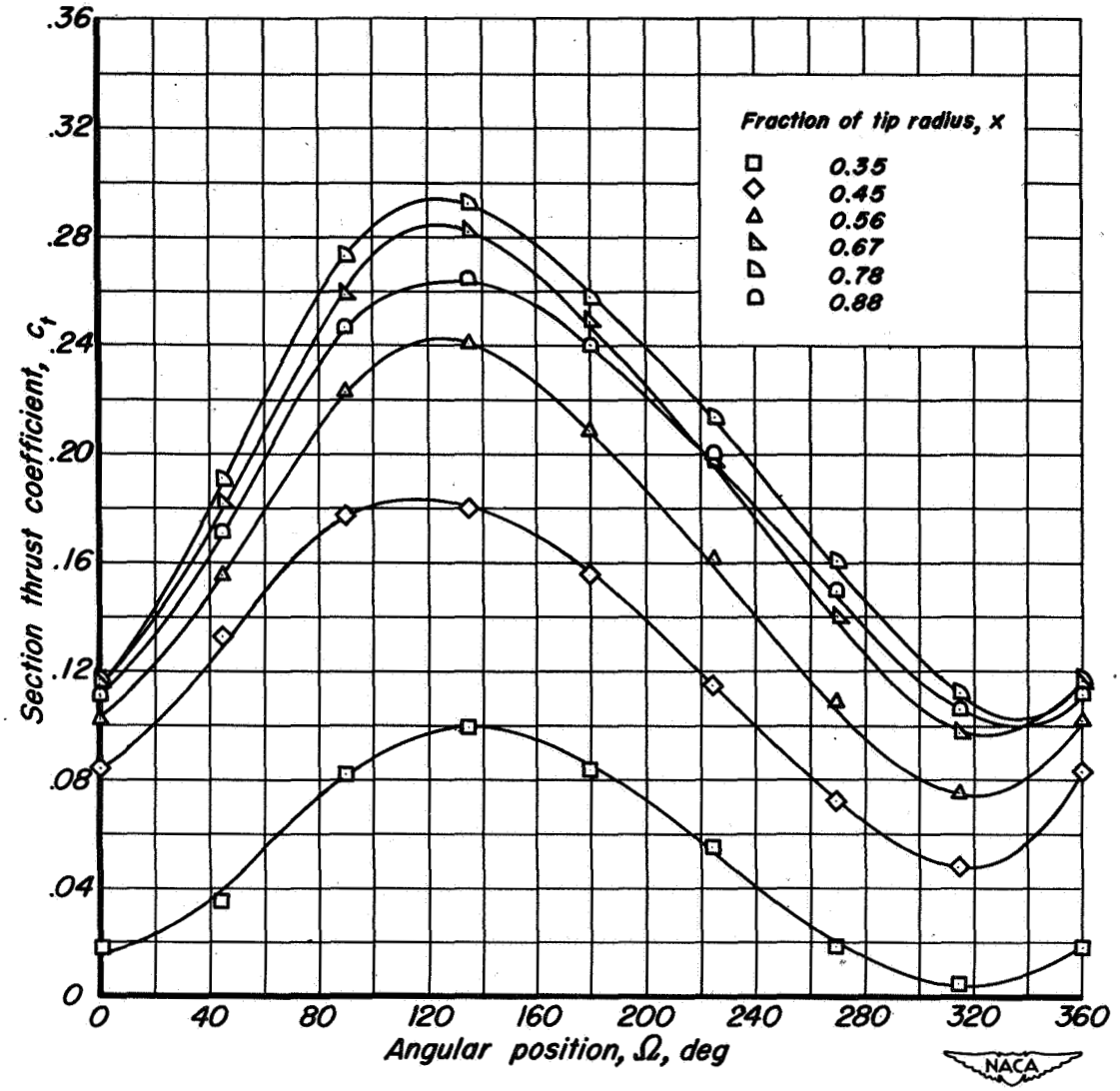

Figure 7.- Measured variation of the section thrust coefficient c_t with angular position Ω. V_0, 165 mph; α_G, 8°; N, 1250 rpm; $\beta_{.75R}$, 20°; four-blade propeller.

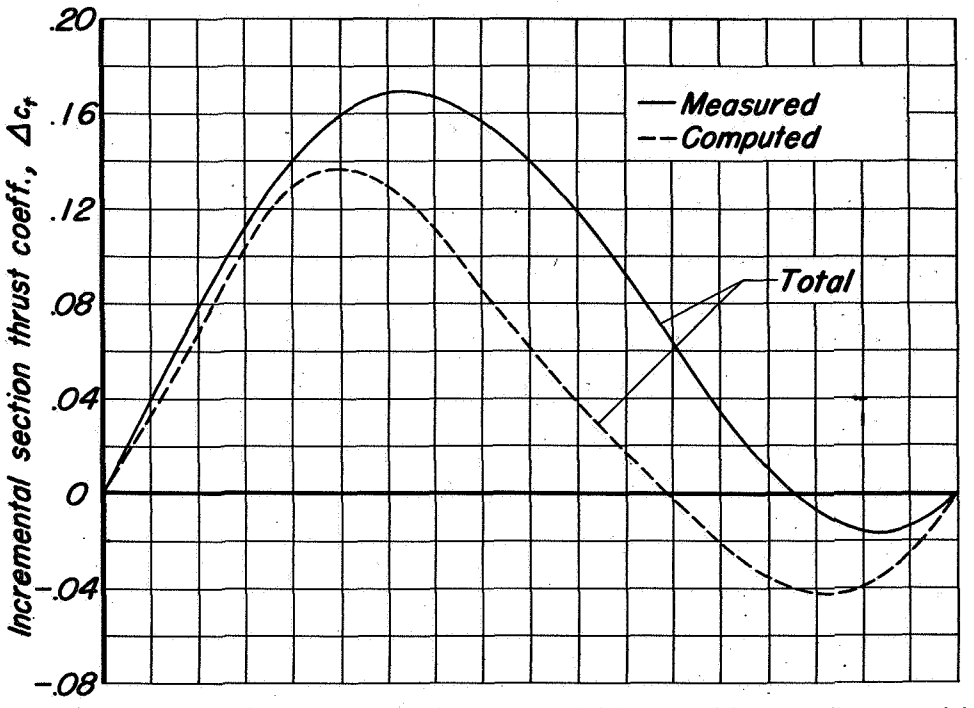

(a) Variation of the total incremental thrust coefficient with angular position.

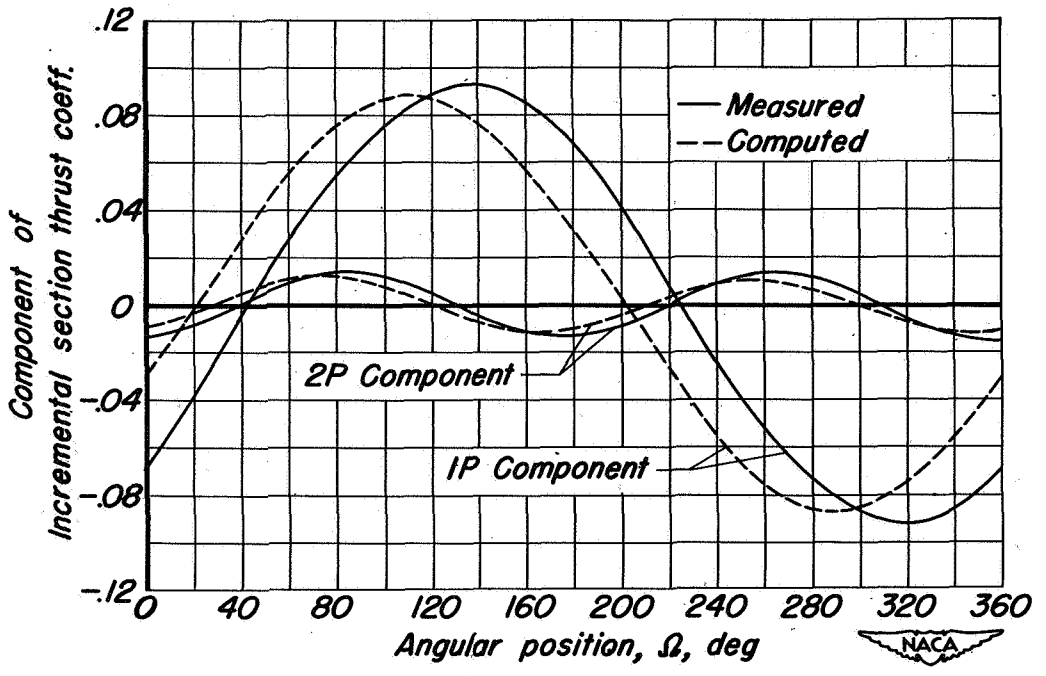

(b) Variation of the first- and second-order components with angular position.

Figure 8. - Comparisons of computed and measured section thrust-coefficient variations at the 0.7-radius station of the propeller. V_0, 165 mph; a_G, 8°; N, 1250 rpm; $\beta_{.75R}$, 20°; four-blade propeller.

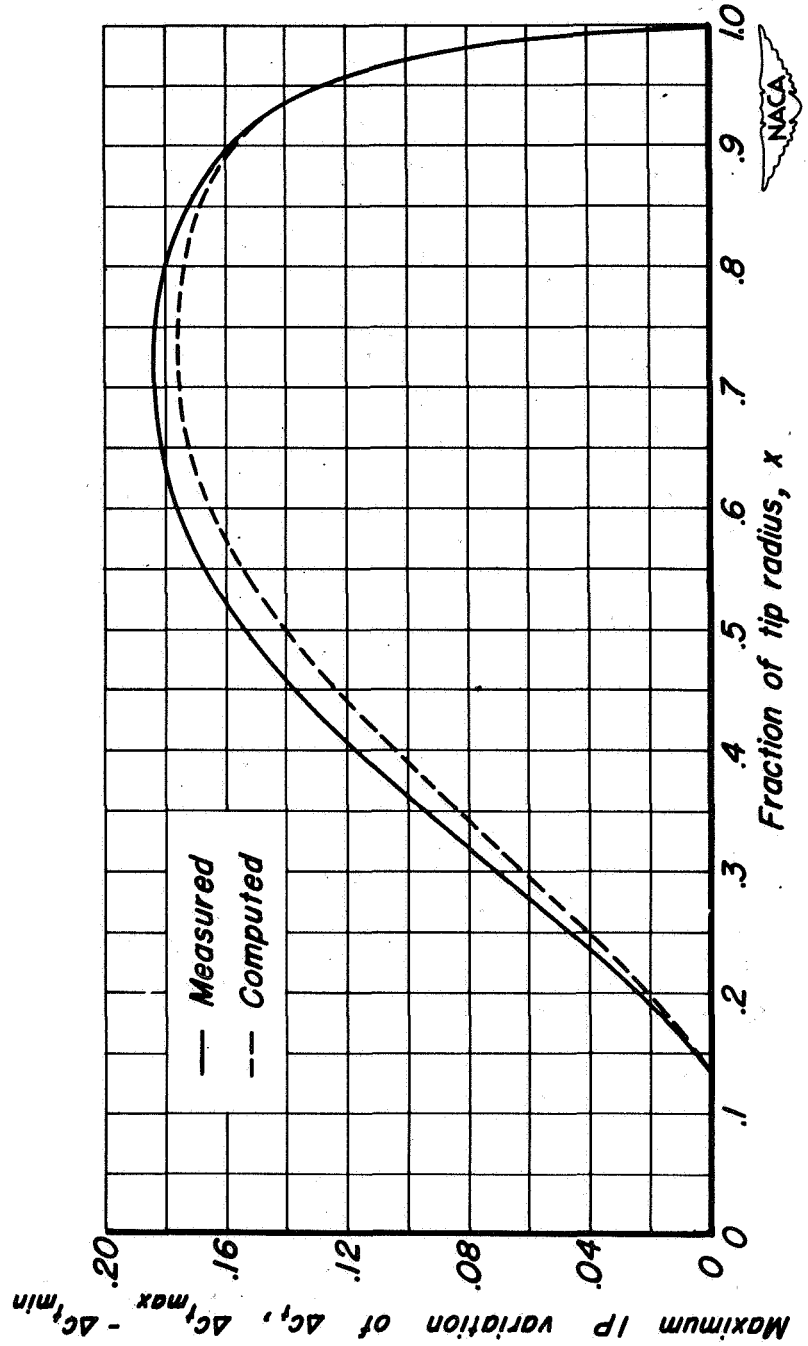

Figure 9. - Comparison of the computed and measured distributions of the maximum variations of the first-order (1P) incremental section thrust coefficient. V_o, 165 mph; N, 1250 rpm; α_s, 8°; $\beta_{.75R}$, 20°; four-blade propeller.

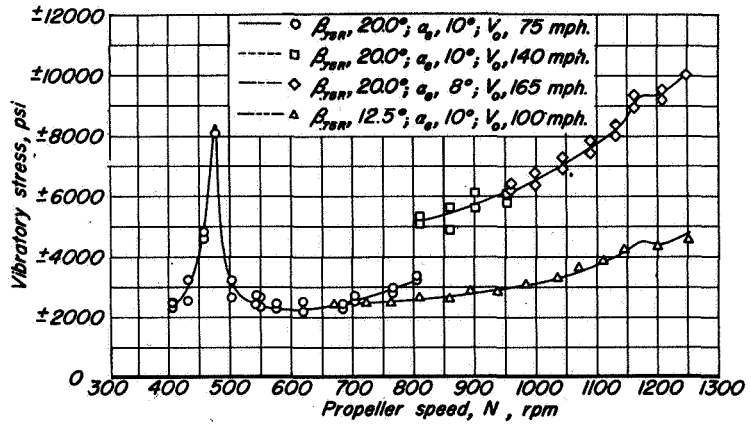

(a) Variation of the total vibratory stress with propeller rotational speed.

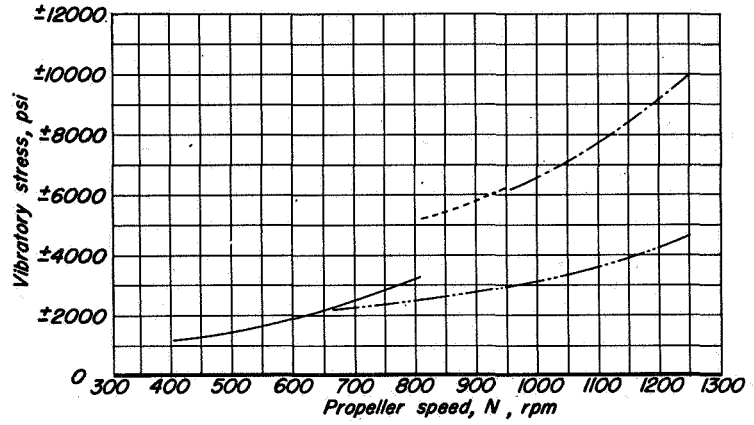

(b) Variation of the first-order (1P) component with propeller rotational speed.

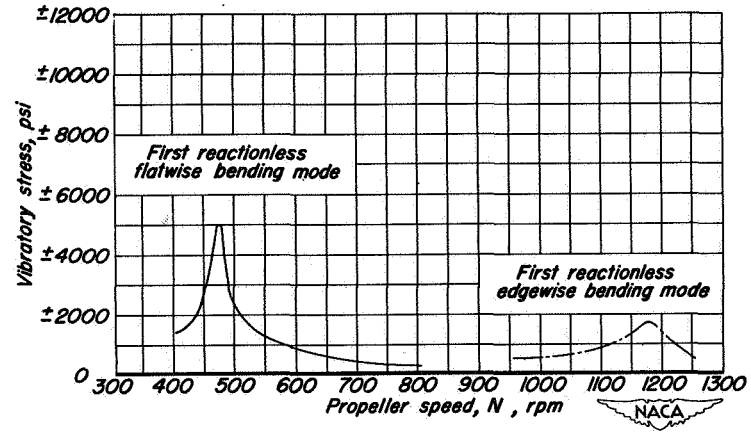

(c) Variation of the second-order (2P) component with propeller rotational speed.

Figure 10. - Vibratory stress measured at the 24-inch radius station; four-blade propeller.

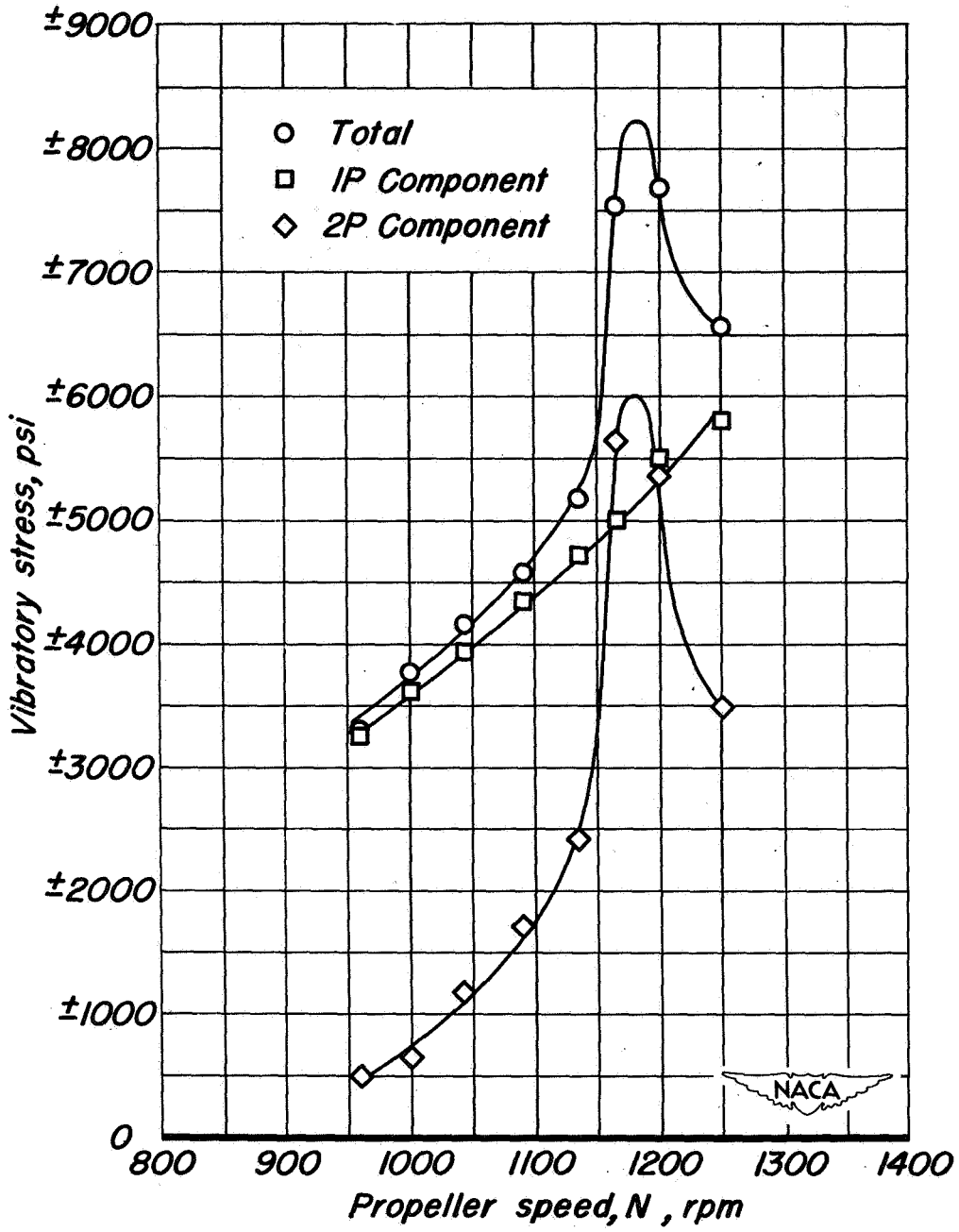

Figure 11. - Vibratory stress measured at shank (11-inch station) V_o, 165 mph; α_6, 8°; $\beta_{.75R}$, 20°; four-blade propeller.

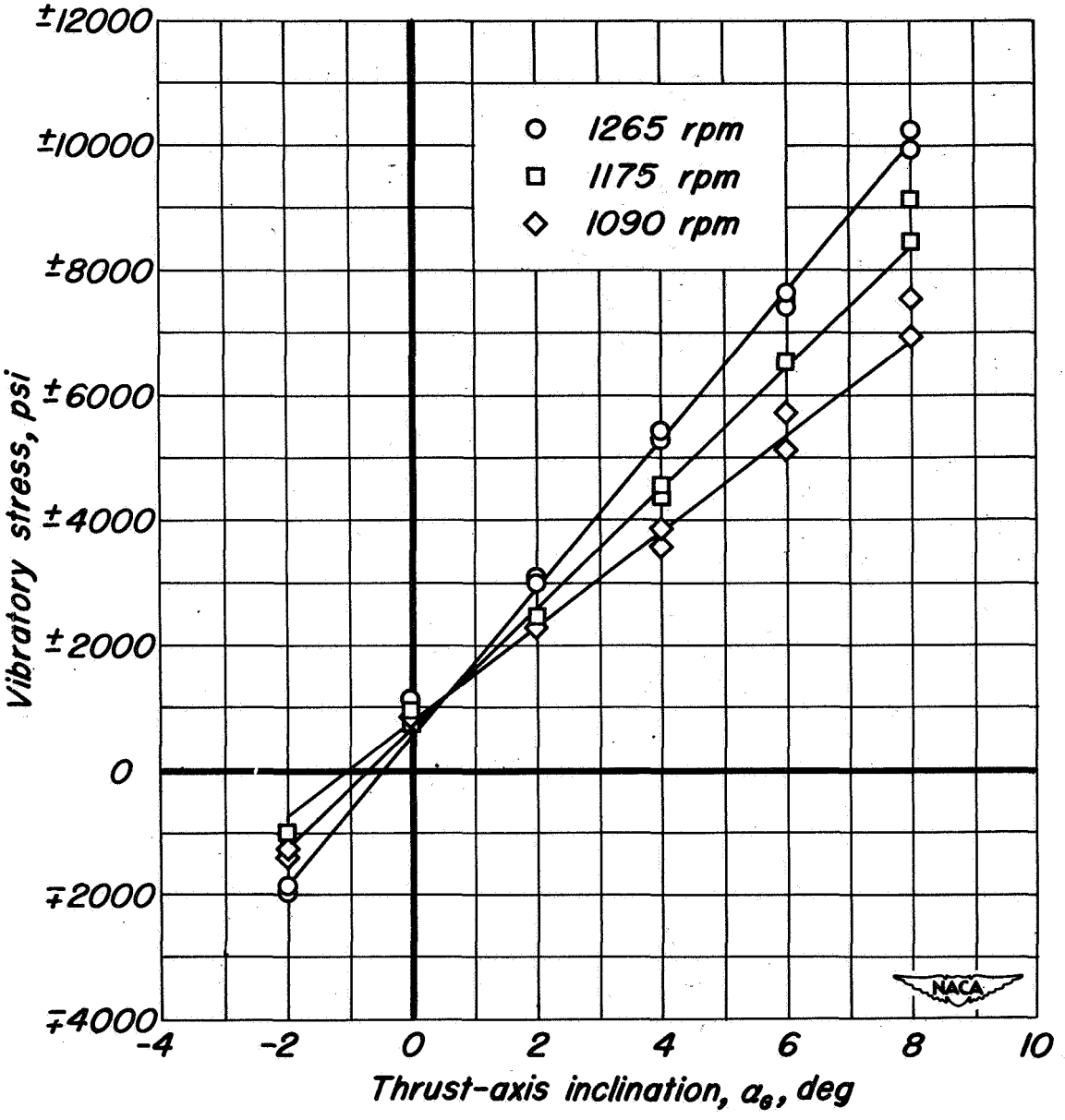

Figure 12.- Variation with thrust-axis inclination of first-order (1P) vibratory stress at the 24-inch station. V_0, 165 mph; $\beta_{.75R}$, 20°; four-blade propeller.

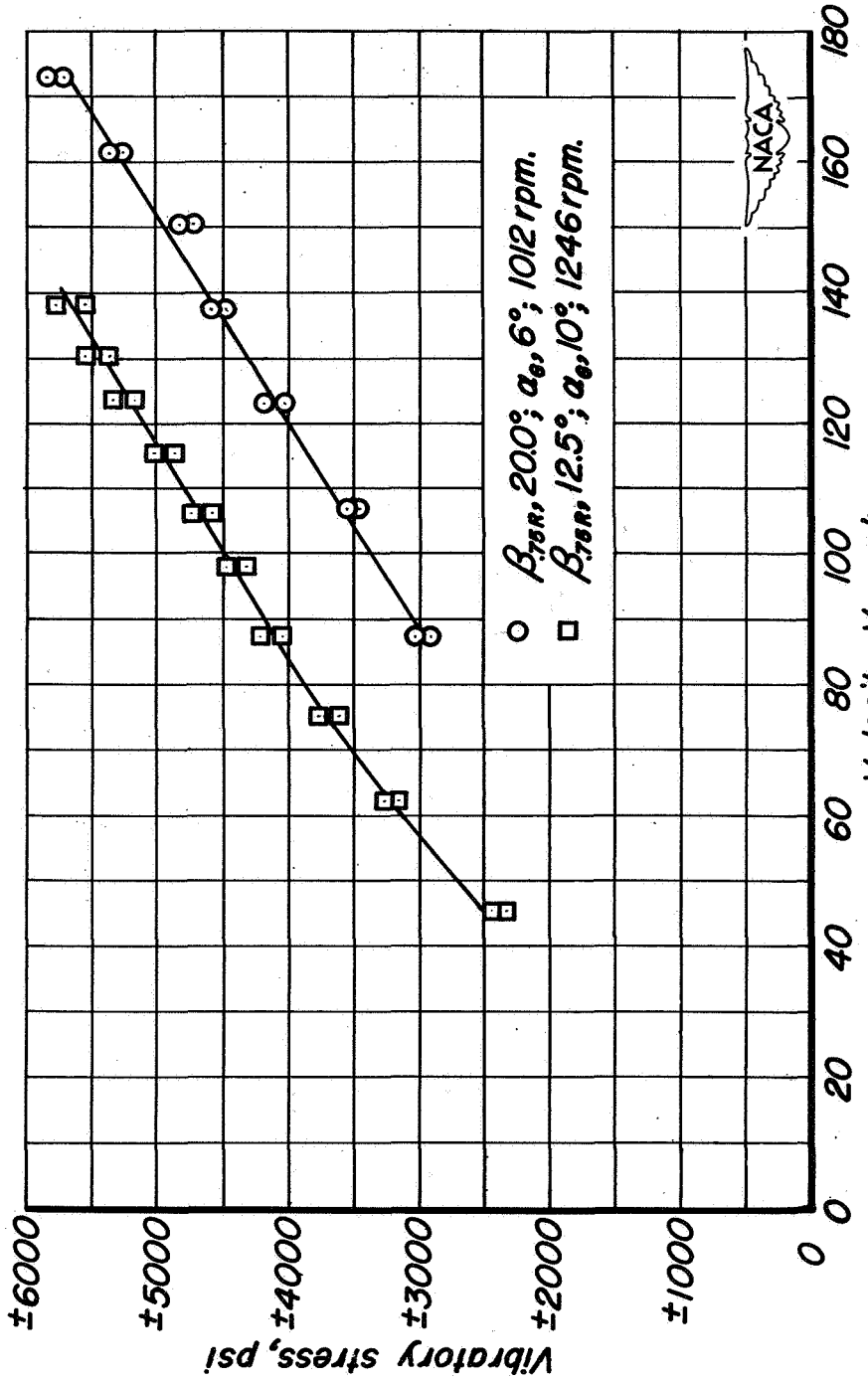

Figure 13.- Variation with stream velocity of first-order (1P) vibratory stress at the 24-inch station. Four-blade propeller.

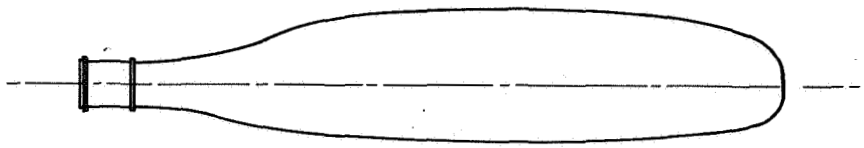

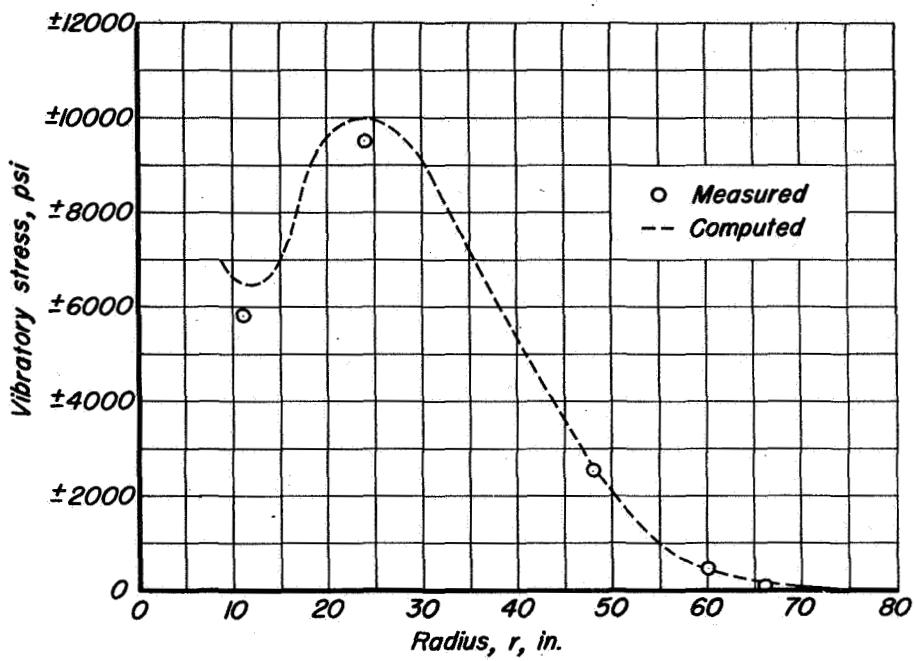

(a) V_o, 165 mph; N, 1250 rpm; a_G, 8°; $\beta_{.75R}$, 20°

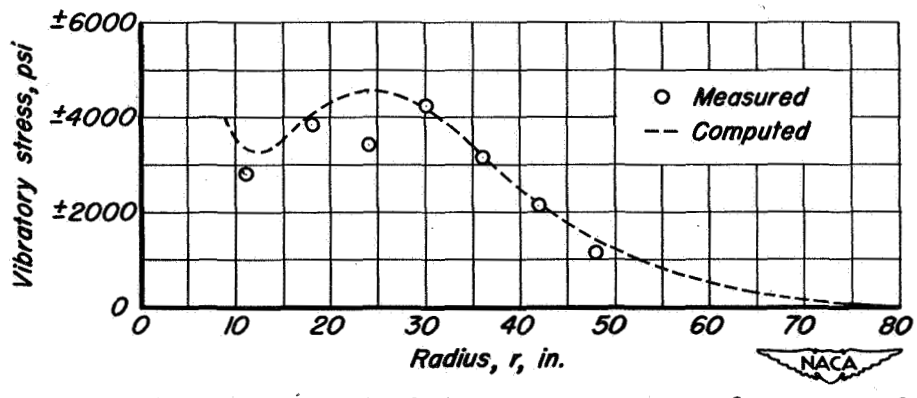

(b) V_o, 100 mph; N, 1250 rpm; a_G, 10°; $\beta_{.75R}$, 12.5°

Figure 14.- Comparison of the computed and measured stress distributions for the four-blade propeller.

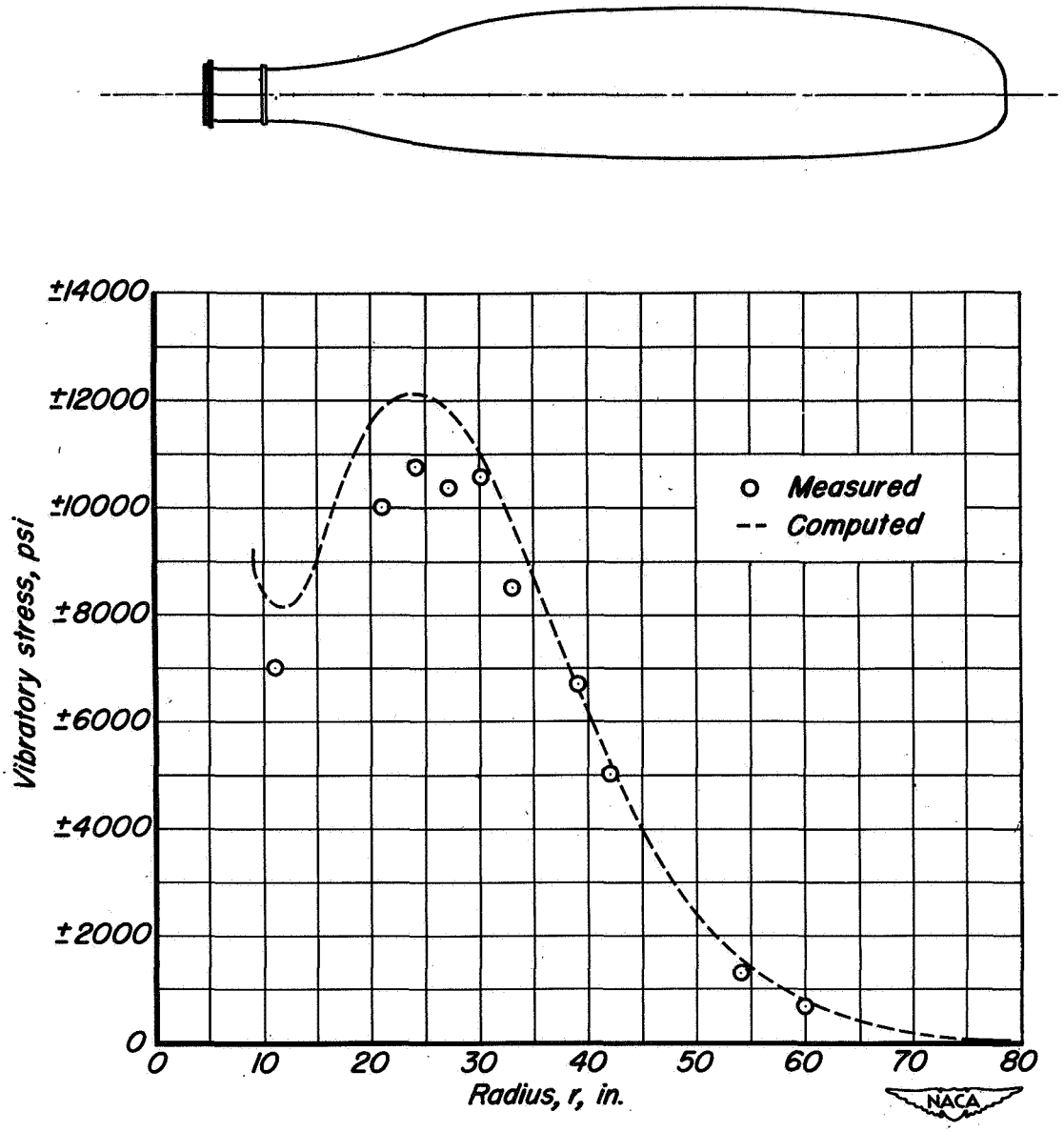

Figure 15. - Comparison of the computed and measured stress distributions for the three-blade propeller. V_0, 165 mph; N, 1250 rpm; a_6, 8°; $\beta_{.75R}$, 20°.